CHEMISTRY
A European Journal

A Journal of
ChemPubSoc Europe

Accepted Article

Title: Triplet state position and crystal field tuning in opto-magnetic lanthanide complexes: two sides of the same coin

Authors: Diogo A Gálico, Riccardo Marin, Gabriel Brunet, Dylan Errulat, Eva Hemmer, Sigoli Aparecido Fernando, Jani Moilanen, and Muralee Murugesu

To be cited as: *Chem. Eur. J.* 10.1002/chem.201902837

Link to VoR: http://dx.doi.org/10.1002/chem.201902837

Supported by
ACES

WILEY-VCH

10.1002/chem.201902837

WILEY-VCH

FULL PAPER

Triplet state position and crystal field tuning in opto-magnetic lanthanide complexes: two sides of the same coin

Diogo A. Gálico, [a],[b]‡ Riccardo Marin,[a]‡ Gabriel Brunet,[a] Dylan Errulat,[a] Eva Hemmer,[a] Fernando A. Sigoli,[b] Jani Moilanen,[c] and Muralee Murugesu[a]*

Abstract: Lanthanide complex-based luminescence thermometry and single-molecule magnetism are two effervescent research fields, owing to the great promise they hold from an application standpoint. The high thermal sensitivity achievable, their contactless nature, along with sub-micrometric spatial resolution make these luminescent thermometers appealing for accurate temperature probing in miniaturized electronics. To that end, single-molecule magnets (SMMs) are expected to revolutionize the field of spintronics, thanks to the improvements made in terms of their working temperature – now surpassing that of liquid nitrogen – and manipulation of their spin state. Hence, the combination of such opto-magnetic properties in a single molecule is desirable in the aim of overcoming, among others, addressability issues. Yet, improvements have to be made through design strategies for the realization of the aforementioned goal. Moving forward from these considerations, we present a thorough investigation of the effect that changes in the ligand scaffold of a family of terbium complexes have on their performance as luminescent thermometers and SMMs. In particular, an increased number of electron withdrawing groups yields modifications of the metal coordination environment and a lowering of the triplet state of the ligands. These effects are tightly intertwined, thus, resulting in concomitant variations of the SMM and the luminescence thermometry behaviour of the complexes. Supported by *ab initio* calculations, we are able to rationally interpret the observed trends and provide solid foundations for the development of opto-magnetic lanthanide complexes.

Introduction

In the quest for novel molecular materials, chemists have made great strides in developing molecules with specific properties. In organic chemistry, for instance, structure directing strategies are exploited to prepare elaborate chemical species. These strategies include exploiting the regioselectivity imparted by groups with an inductive effect on the charge distribution of the molecular scaffold to which they are bound. However, the consequences of the inductive effect exerted by specific moieties do not end there. On a more general level, the electron cloud distribution governs a number of properties of the chemical species, which encompass, but are not limited to, conductivity,[1-3] reactivity,[4, 5] as well as catalytic [6-8] and optical activity.[9-13]

In the context of metal complexes, the choice of ligands containing different atoms – thus possessing a distinctive electron cloud distribution – enables the preparation of chemical species with tailored properties. Indeed, the interaction between purposely designed ligands and the selected metal centre is pivotal to ensure features such as sensitized photoluminescence[14, 15] and magnetic anisotropy.[16-19] Often, small differences in the ligand scaffold can lead to important changes in the features of the final complex despite maintaining nearly identical metal coordination environment. Thus, a thorough understanding of the influence that the ligand scaffold has on the properties of a metal complex is a powerful tool for the design of multifunctional molecular materials.

Herein, we embrace this notion and rationalize the concomitant effects that the degree of fluorination has on the structure, luminescence thermometry behaviour, and magnetic properties of a family of dinuclear terbium complexes built upon diketonate-based ligands. Amongst the lanthanide ions, terbium (in its trivalent form – Tb^{3+}) is especially appealing because of the possibility to harness its properties both from a magnetic and optical standpoint. Countless examples of Tb^{3+}-based single-molecule magnets (SMMs)[20-24] as well as luminescent complexes of the same ion[12, 15, 25, 26] have been reported. These luminescent species have been applied extensively as probes in assays[25, 27, 28] and for lighting purposes.[29-31] More recently, their application as luminescent thermometers is being widely explored[32-34] with outstanding results in terms of thermal readout performance.[35-38] However, to date, no study investigates the concurrent influence of the ligands on the SMM and luminescent thermometer performance of opto-magnetic systems.

Recently, we demonstrated for the first time that Dy^{3+}[39] and Yb^{3+}[40] SMMs can simultaneously act as luminescent thermometers. Thus, the apparent significance of Tb^{3+} complexes as multifunctional species is at the base of this study, which unveils the intermingled effects that different ligands have on the coordination geometry of the metal centre and the sensitization of its photoluminescence. The results show that the multifunctional complexes can be premeditatively endowed with better luminescence thermometry or SMM properties *via* a fine tuning of the ligand scaffold. Such rationalization of the synergistic impact of the ligands on the optical and magnetic properties of the

[a] Dr. D. A. Gálico, Dr. R. Marin, G. Brunet, D. Errulat, Prof. E. Hemmer, Prof. M. Murugesu
Department of Chemistry and Biomolecular Sciences, University of Ottawa, Ottawa, Ontario K1N 6N5, Canada.
E-mail: M. Murugesu@uottawa.ca
[b] Dr. D. A. Gálico, Prof. F. A. Sigoli
Institute of Chemistry, University of Campinas, UNICAMP, P.O. Box 6154, Campinas, Sao Paulo 13083-970, Brazil.
[c] Prof. J. Moilanen
University of Jyväskylä, Department of Chemistry, Nanoscience Centre, P.O. Box 35, FI-40014, Finland.

Supporting information for this article is given via a link at the end of the document.

complexes is unprecedented, and paves the way for the design of multifunctional opto-magnetic molecular materials.

Results and Discussion

Structural studies

To achieve our goal of isolating tuneable multifunctional opto-magnetic molecular materials, we focused on a family of dinuclear Tb^{3+} complexes based on our previously reported $[Ln_2(bpm)(tfac)_6]$ system.[26] More specifically, three complexes were isolated with the following chemical composition/formula, $[Tb_2(bpm)(acac)_6]$, (**Tb-acac**); $[Tb_2(bpm)(tfac)_6]$, (**Tb-tfac**) and $[Tb_2(bpm)(hfac)_6(H_2O)_2]$, (**Tb-hfac**,); where bpm: bipyrimidine; acac: acetylacetonate; tfac: 1,1,1-trifluoroacetylacetonate; hfac: hexafluoroacetylacetone.

These molecules were obtained using slightly modified reported procedures.[41, 42] This family allows us to fine-tune the electronic structure *via* the terminal diketonate-based ligands while retaining essentially the central $\{Tb_2bmp\}^{6+}$ core intact. In this way, it was possible to systematically examine the optical and magnetic properties affected by the electron withdrawing groups of the terminal ligands. Molecular structures were obtained using single-crystal X-ray crystallography and they are shown in Figure 1. Selected bond-distances and angles are presented in Table S1. The dinuclear Tb_2 complexes are composed of two Tb^{3+} ions bridged by a planar 2,2'-bipyrimidine (bpm) ligand. The remainder of the coordination environment is occupied primarily by beta-diketonate (from here on, simply diketonate) ligands with varying electron withdrawing groups, *i.e.*, acetylacetonate (acac). It is noteworthy that the metal ions in **Tb-acac** and **Tb-tfac** complexes adopt an eight coordination environment while Tb^{3+} ions in the **Tb-hfac** complex adopt a nine coordination environment. In the latter system the additional coordination environment is occupied by a water molecule. This is likely due to the fact that the highly electron withdrawing nature of the $hfac^-$ ligands induces an electron poor region around the metal, which subsequently promotes the coordination of additional ligand molecules (H_2O) to stabilize the **Tb-hfac** complex. This change in the coordination environment has an important impact on the physical properties of the compounds (*vide infra*). In **Tb-acac** and **Tb-tfac** the metal centres showcase respectively a triangular dodecahedral (D_{2d}) and square antiprismatic (D_{4d}) coordination geometry (Table S2). Notably, in **Tb-hfac**, two crystallographically independent dinuclear species are present, namely **Tb-hfacA** and **Tb-hfacB**, which display a slightly different degree of distortion of the same coordination geometry (C_{4v} - Table S3). The presence of bound water in the latter complex was also confirmed *via* Fourier transform infrared (FTIR; Figure S1) and thermogravimetry (TG; Figure S2) analysis.

Spectroscopic studies and luminescence thermometry

The existence of different Tb^{3+} coordination geometries in the three complexes has a substantial impact on both SMM and optical performances of the compounds (*vide infra*). In this vein, the UV-triggered photoluminescence of the investigated systems is guaranteed by the sensitization of the ligands (Figure 2 and Figure S3). The most common sensitization mechanism in lanthanide complexes entails a ligand-centred photon absorption followed by electron relaxation to the lowest triplet state (T_1) of the ligand scaffold.[14] From there, energy transfer (ET) to the Tb^{3+}: $^5D_4$ emitting level eventually occurs. In general, the T_1 energy of a specific diketonate moiety does not vary considerably from complex to complex. For the selected diketonates the position of T_1 correlates with the stabilization imparted by the electron withdrawing groups (*i.e.*, fluorine atoms).

The values are approximately 24800 ($acac^-$), 22700 ($tfac^-$), and 22200 cm^{-1} ($hfac^-$) (Figure 2B).[33, 41, 43, 44] Since the Tb^{3+}: $^5D_4$ level falls at approximately 20570 cm^{-1}, the energy differences with the T_1 of the diketonates are suitable for an efficient ligand-to-metal ET in all these complexes.[14] However, while in **Tb-hfac** and **Tb-tfac** this ET preferentially takes place from the diketonate, in **Tb-acac**, bpm (T_1 – 23350 cm^{-1}) plays also a role in the sensitization (Figure S4).[43] Indeed, a dim Tb^{3+} emission was observed at room temperature for **Tb-acac**. The other two complexes featured a brighter emission at room temperature, **Tb-hfac** exhibiting a stronger emission intensity compared to **Tb-tfac**. The bright emission of **Tb-hfac** stems from the combination of the aforementioned favourable relative position of the energy levels and a less symmetrical coordination environment

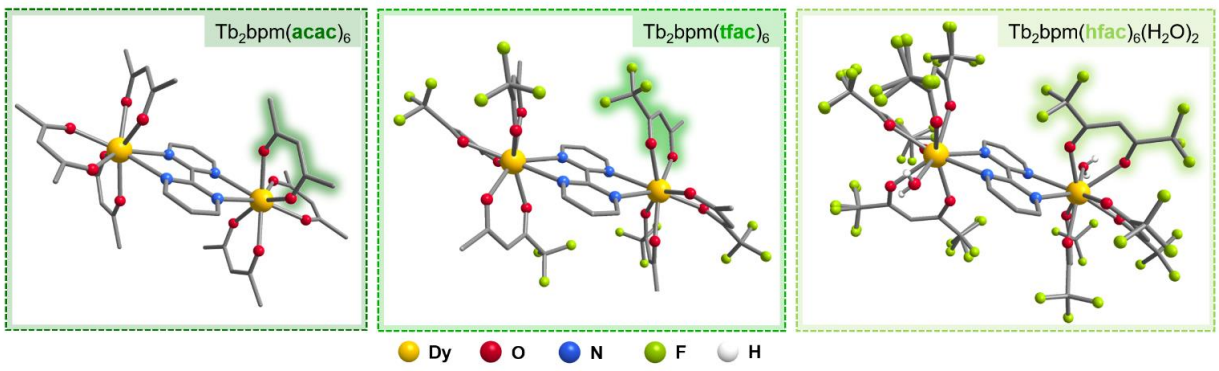

Figure 1. Coordination environment of the asymmetrical unit of $[Tb_2bpm(acac)_6]$, (**Tb-acac**) (left), $[Tb_2bpm(tfac)_6]$ (**Tb-tfac**) (middle) and $[Tb_2bpm(hfac)_6(H_2O)_2]$ (**Tb-hfac**) (right) highlighting the electron withdrawing groups of the diketonate ligands. Colour code: orange – Tb, red – O, blue – N, green – F. Only the H atoms of water are shown (white).

10.1002/chem.201902837

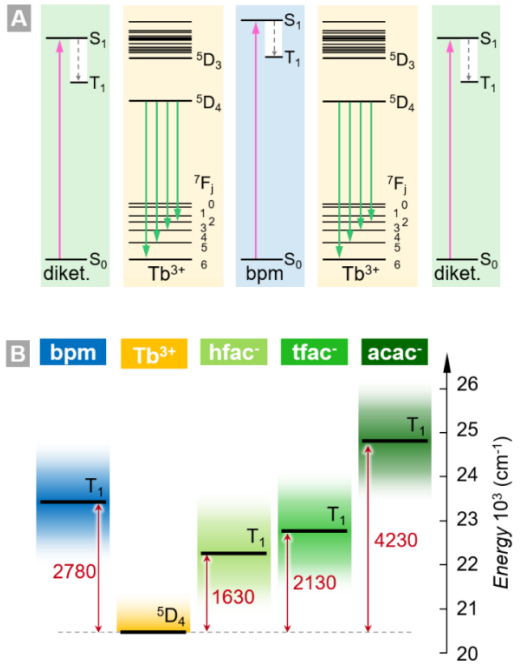

Figure 2. Generic energy level scheme (A) for the investigated family of complexes (diket. = diketonate). In B, the relative position of the triplet states of the ligands and Tb^{3+} emitting level ($^5D_4$) is presented. Values in B are obtained from the literature cited in the main text.

(nine-coordinate) compared to **Tb-tfac** (eight-coordinate). The brighter emission observed for **Tb-hfac** was corroborated by the measured overall quantum yield values upon excitation *via* ligand (Figure S5). The obtained values for **Tb-hfac** and **Tb-tfac** were 59.8 ± 0.9 and 8.9 ± 0.2%, respectively. For **Tb-acac** the obtained value was below 1%.

These differences in the optical properties were further explored testing the temperature-dependent behaviour of the emission of the three complexes. All of them featured bright emission at liquid nitrogen temperature (Figure S3) due to a reduced density of high-energy phonons (responsible for non-radiative de-excitation mechanisms) and minimization of back-ET phenomena at that cryogenic regime. A temperature increase led to the emission quenching of **Tb-acac** and **Tb-tfac** (more abrupt for the former, gradual for the latter), while **Tb-hfac** retained a better brightness up to 323 K. Above this threshold, the measurements were not possible for this complex, due to the irreversible loss of the coordinated water molecule (occurring above 50 °C, *i.e.*, 323 K – Figure S2) leading to a loss of structural integrity. In Tb^{3+}-containing species, the symmetry of the coordination environment can be spectroscopically probed by taking the ratio (R) between the $^5D_4 \rightarrow {}^7F_5$ and $^5D_4 \rightarrow {}^7F_6$ transitions.[33] These display significant forced electric and magnetic dipole nature, respectively, the intensity of the former being sizably influenced by the symmetry of the coordination environment. Hence, the higher the R value, the more asymmetric/distorted the coordination geometry is expected to be. More precisely, the odd-terms in the crystal-field Hamiltonian (B_q^k, k = 1, 3, 5 and 7) in Wybourne's formalism are responsible for the intensity of forced electric dipole transitions.[45] Moreover, a higher number of odd-terms results in a greater dependence of these transitions upon distortions of the coordination geometry. In general, in high-symmetry coordination geometries, fewer odd-terms are present (see for example the Appendix 3 of reference [46]), hence a lesser dependence upon distortion is expected. For the three complexes under study, the trend of R (**Tb-hfac** > **Tb-tfac** > **Tb-acac**; Figure S6) well correlates with the absolute intensity trend (Figure S3D). Indeed, as opposed to **Tb-acac** and **Tb-tfac** (featuring more symmetrical coordination environments), **Tb-hfac** shows a marked thermal dependence of R, which can explain the intensity increase observed for this compound at low temperatures.

The differences between the three complexes are even more significant when assessing the performance of the compounds as luminescent thermometers (Figure 3; calculations in the Supporting Information). When selecting a luminescent thermometer, one of the more robust thermal parameter to consider is the luminescence lifetime (τ) of the energy level from which the transition associated with the monitored emission stems.[47-49] Although usually requiring a rather sophisticated

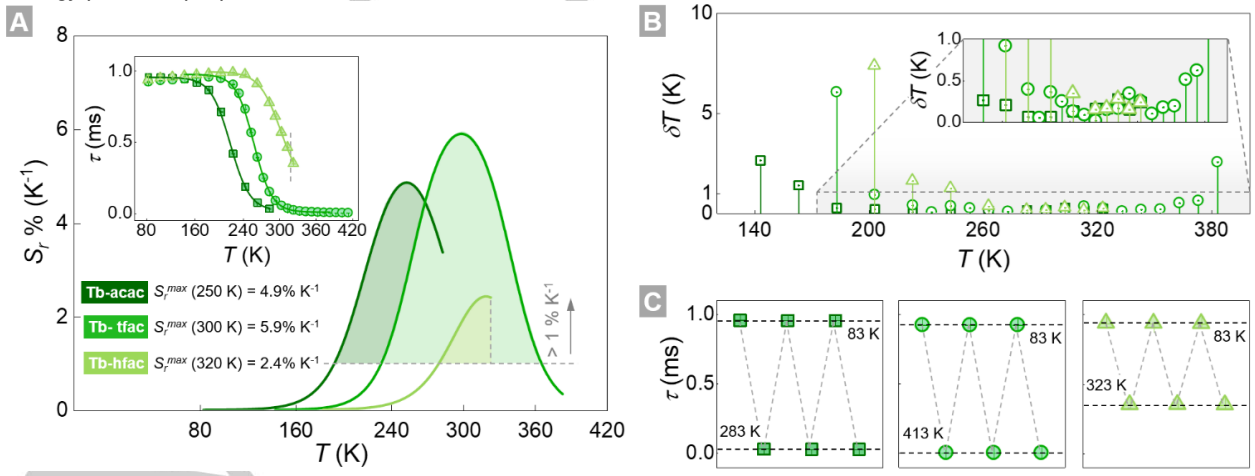

Figure 3. Relative thermal sensitivity S_r (A) as obtained from the fitting procedure of the lifetime values according to a Mott-Seitz model (inset in A). Temperature uncertainties δT (B) and repeatability tests (C).

detection system, this parameter allows to overcome the shortcomings related with non-ratiometric intensity-based methods (*e.g.*, intensity and concentration variations, along with power fluctuations of the excitation source).[48-50] The observed trend of τ (inset in Figure 3A), as obtained from the fit of the decay curves (Figure S7), is similar to the one discussed for the absolute intensity (Figure S3D). In the case of **Tb-acac**, the intensity differs more noticeably from the lifetime trend, which is a result of the aforementioned temperature-dependent change of the excitation spectra (see also discussion below). At low temperature, the measured τ is approximately 1 ms for all the studied complexes. This value decreases to few microseconds approaching room temperature for **Tb-acac** and **Tb-tfac**. In the case of **Tb-hfac**, τ decreases to approximately 350 µs at 323 K and random fluctuations of its value (not shown here) were observed above this temperature due to the previously mentioned loss of coordinated water. The lifetime value drop observed in all complexes follows from the depopulation of the emitting level and the room temperature value is in agreement with the measured absolute quantum yield values.

Often, this behaviour can be understood considering a two-state system, with a thermally activated back-ET from the emitting state (here Tb^{3+}: $^5D_4$) to a higher energy level (ligands). The Mott-Seitz model mathematically describes this interaction by considering the radiative and non-radiative transition probability of the emitting state (see Equation S1).[51, 52] Hence, the temperature-dependent lifetime shortening could be quantitatively interpreted by applying this model. The activation energies obtained by fitting the experimental data (inset in Figure 3A) using Equation S1 were quite dissimilar from the expected energy differences between Tb^{3+}: $^5D_4$ and the closest ligand T_1 in each complex (Figure 2B). The higher values observed for **Tb-tfac** and **Tb-hfac** (3250 and 2980 cm^{-1}, as compared to the expected 2130 and 1630 cm^{-1}) result from the energy minima position of the considered levels, which are centred at different configurational coordinates. This leads to an intersection between the potential wells at energies higher than the difference between the minima,[53, 54] thus resulting in a higher thermal barrier for the ET. Due to the small energy difference between the diketonates and bpm T_1, also a back-ET between the ligands is expected to contribute to the observed trend of τ (inset in Figure 3A) as well as of the absolute intensity (Figure S3). The low activation energy found for **Tb-acac** (2275 cm^{-1}) indicates that the Mott-Seitz model is not suitable to describe the behaviour of this system. Although Equation S1 still provides a good fit of the experimental data (see inset in Figure 3A), the shortening of Tb^{3+}: $^5D_4$ lifetime can be explained considering a thermally-induced depopulation of bpm T_1 state. This overall leads to a less efficient population of Tb^{3+} emitting level at high temperatures. This interpretation is also corroborated by the change in the excitation spectrum of the complex passing from cryogenic to room temperature, showing a reduced contribution of bpm (feature centred around 350 nm) to the sensitization of the lanthanide emission (Figure S4).

Ultimately, the different behaviour featured by the three complexes translated to different ranges of usability of the luminescent thermometers (Figure 3A). The maximum relative thermal sensitivity (S_r) displayed by the compounds – obtained using Tb^{3+}: $^5D_4$ lifetime as the thermal parameter, according to the guidelines given by Carlos *et al.*[55] – shifted from 250 to 320 K following the order **Tb-acac**, **Tb-tfac**, **Tb-hfac**. All thermometers showed S_r > 1% K^{-1} over an extended temperature range, along with an associated uncertainty, δT, well below 1 K (Figure 3B) and repeatability above 99% (Figure 3C). Nevertheless, **Tb-tfac** outperformed the other complexes with a maximum sensitivity of 5.7% K^{-1} at 300 K – amongst the highest values reported for lanthanide complex-based luminescent thermometers.[56] **Tb-acac** was apt for a lower-temperature operation, whilst **Tb-hfac** showed a more limited usability due to the constraints imposed in terms of maximum operating temperature (*i.e.*, 323 K) by the labile water molecule in the Tb^{3+} coordination sphere.

Overall, the luminescent properties of the complexes were mainly influenced by the position of the lowest lying triplet state of the ligand scaffold. This is influenced by the presence of an increasing number of electron withdrawing groups (*i.e.*, fluorine ions) in the diketonate. In turn, this leads to an energy stabilization of the system and, thus, a lowering of the position of the triplet state of this moiety. The energy difference between Tb^{3+} emitting state ($^5D_4$) and the closest triplet state (either of bpm or the diketonate) both influences the brightness of the complex emission and governs its behaviour as a luminescent thermometer. Instead, the coordination environment of the metal centre only plays a complementary role in determining the absolute emission intensity of the complex. This is reflected in the temperature dependency of the emission intensity of **Tb-hfac** at low temperatures, where a more pronounced thermally-induced distortion of the coordination geometry is observed.

Single-molecule magnet behaviour

As demonstrated above, electron withdrawing moieties within the ligand scaffold can have a drastic effect on both the emission intensity and on the thermometric capabilities. With this in mind, we sought to investigate the effect of such groups on their magnetic behaviour, with a particular focus on complexes based on non-Kramers ions, such as Tb_2 SMMs. Our recent work in this regard has shown that the stabilization of ground Kramers doublet and the reorientation of the magnetic anisotropy axes can lead to significant improvements in the energy barrier (U_{eff}).[16, 57] In doing so, we are able to identify the key points for a design strategy that optimizes the performance of the complex from both a magnetic and optical perspective.

To probe the magnetic behaviour of the three complexes, direct current (dc) magnetic susceptibility measurements were carried out in the temperature range of 1.9-300 K and under an applied field of 1000 Oe (Figure 4). The room temperature χT values of 24.78, 23.14, and 24.33 cm^3 K mol^{-1} for **Tb-acac**, **Tb-tfac**, and **Tb-hfac**, respectively, are in good agreement with the expected value of 24.38 cm^3 K mol^{-1} for two non-interacting Tb^{3+} ions.[58, 59] The χT product remains relatively constant for all complexes until ~100 K, where we begin to observe a slight decrease attributed to the thermal depopulation of Stark sublevels. The sharper decreases at low temperatures (below 10 K) have been well investigated, and are typical of weak antiferromagnetic exchange interactions between Tb^{3+} and/or significant magnetoanisotropy.[60, 61]

10.1002/chem.201902837

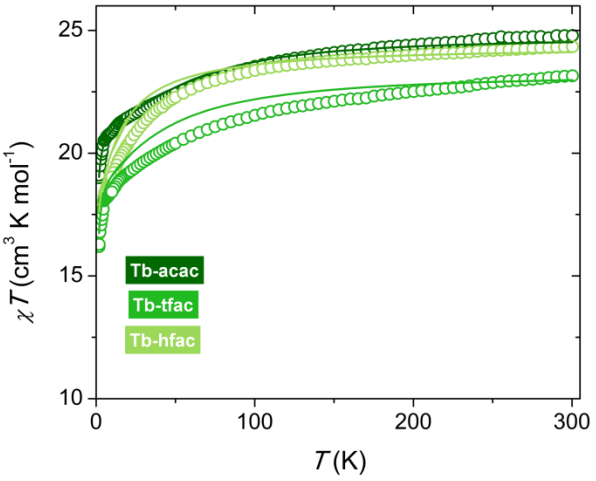

Figure 4. Temperature dependence of the molar susceptibility (spheres), plotted as χT, for all compounds, collected under an applied field of H_{dc} = 1000 Oe and comparison to their respective calculated magnetic susceptibility (solid lines).

The field dependence of the magnetization (*M vs*. *H*) (Figures S8 and S9), exhibits a rapid increase at low fields (< 2 T) and approaches saturation at higher fields (7 T). The lack of Tb^{3+}-Tb^{3+} magnetic interactions are further highlighted by the lack of an S-shaped curve, and point towards a complex in which the metal ions behave individually.

To confirm the experimental conclusions drawn from the dc magnetic susceptibility measurements, we calculated the total intramolecular magnetic coupling constant (J_{intra_tot}) for all investigated complexes through *ab initio* calculations by taking into account the contributions of the exchange (J_{intra_exh}) and dipolar (J_{intra_dip}) interactions to the total magnetic coupling (see computational details). For **Tb-acac,** we also estimated the magnitudes of intermolecular dipolar coupling constants J_{inter_dip}. The calculations revealed that in all investigated complexes, the total intramolecular coupling J_{intra_tot} between Tb^{3+} ions is antiferromagnetic and weak (less than -1.0 cm^{-1}) with a slightly larger contribution from the exchange (J_{intra_exh}) than dipolar (J_{intra_dip}) coupling (Table S4). For **Tb-acac**, The calculated values of J_{inter_dip} indicate that intermolecular dipolar coupling between neighbouring Tb^{3+} ions, that lie within 15 Å from the central Tb^{3+} ion, are weak (less than ± 0.3 cm^{-1}). However, the order of the magnitude of the intermolecular dipolar coupling constants is similar with the magnitude of the intramolecular dipolar coupling constants (Table S4 and S5). Thus, the calculated coupling constants not only suggest that the intramolecular coupling between Tb^{3+} ions are weak and antiferromagnetic in all investigated complexes, but they also show that the intermolecular dipolar couplings influence almost as equally as the intramolecular magnetic interactions on the magnetic properties of the investigated complexes.

To investigate possible SMM-like behaviour, the described compounds were investigated by alternating current (ac) magnetic susceptibility measurements and by probing the slow magnetic relaxation dynamics. In all cases, the application of an applied external dc field was necessary to observe an ac signal, indicating that quantum tunnelling of the magnetization (QTM) plays an important role in circumventing the reversal of the magnetization through thermally-activated processes. To determine the effect of an applied field on the magnetic relaxation times, the frequency dependence of the out-of-phase (χ') magnetic susceptibility under fields ranging from 0 to 5800 Oe for **Tb-acac** – the best performing SMM herein investigated – was measured (Figure 5). It is clear from this data that two magnetic relaxation modes are operative and that there is a strong field dependence on the observed behaviour.

Fitting these data to a two-component Debye model allows the extraction of the relaxation times associated to each relaxation process (Table S6).[62, 63] Next, the τ^{-1} *vs*. *H* plot allows the determination of the contribution of field-dependent magnetic relaxation processes, namely direct, Raman and QTM. While an initial increase in the magnetic relaxation times (τ) can be observed up to 1400 Oe, a decrease upon higher fields is a clear indicator of the direct process becoming predominant for both low and high frequency processes (Figure S10).[64, 65] A suitable fit of the low frequency process was obtained by including contributions from the direct and QTM processes (Equation 1). In contrast, the high frequency process, which is also thermally-activated, was fit by considering contributions from direct and QTM processes, in addition to a constant representing the Orbach process (Equation 2). The addition of a Raman term in both cases did not produce a successful fit of the data. The results of the best-fit are summarized in Table S7 and shown in Figure S11.

$$\tau^{-1} = AH^2T + (B_1/1+B_2H^2) \quad (1)$$

$$\tau^{-1} = AH^2T + (B_1/1+B_2H^2) + C \quad (2)$$

Next, the temperature dependence of the ac magnetic susceptibility was probed under a static field of 1000 Oe (Figure 5). This serves to circumvent QTM and obtain longer relaxation times. Again, we observed two well-isolated magnetic relaxation processes. The low frequency process only appears at lower temperatures and does not exhibit a frequency-dependent signal, confirming that the QTM and/or direct processes are predominant. The high frequency process however, is observable in the full 1.9-10 K range and is seen shifting to lower frequencies upon decreasing the temperature. This is a clear indication of slow relaxation of the magnetization that is thermally activated.[24, 66] Applying the same two-component Debye model to this data yields the relaxation times for both low and high frequency processes (Table S8).

An initial approximation of the energy barrier for the high frequency process can be estimated by a linear fit of the high temperature region using an Arrhenius law yielding U_{eff}/k_B = 27.17(2) K and τ_0 = 4.42(6) × 10^{-6} s (Figure 6). To more comprehensively estimate the energy barrier, the τ^{-1} *vs*. *T* data was fit to an equation encompassing direct, QTM, and Orbach processes (Equation 3). The values previously determined for the direct and QTM terms were inserted leaving only two parameters to fit, thereby avoiding overparameterization.

10.1002/chem.201902837

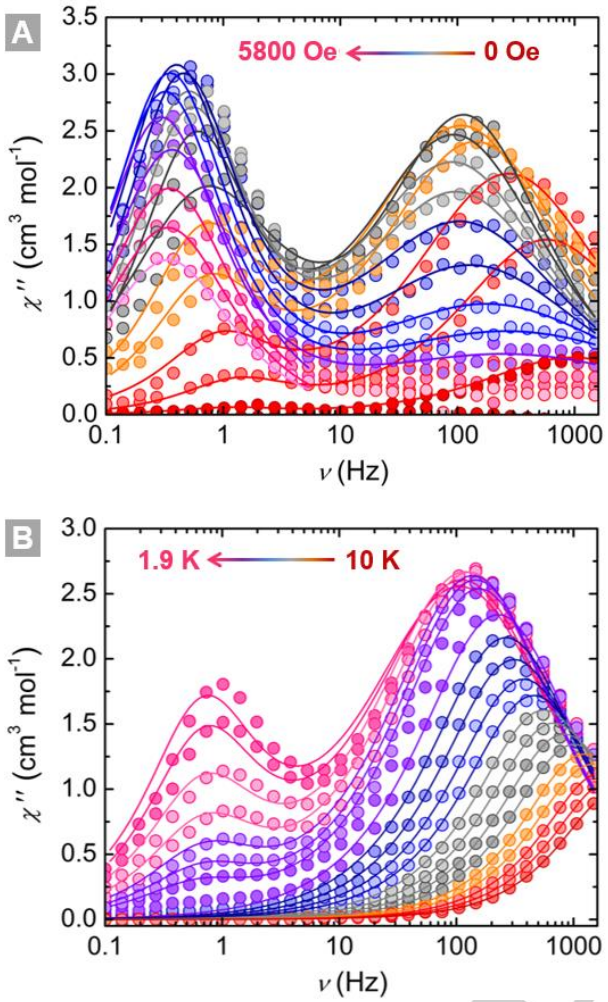

Figure 5. Field (A) and temperature (B) dependence of the χ'' magnetic susceptibility for Tb-acac collected under an applied dc field of 1000 Oe. The variable field data was collected at 2 K, while the temperature dependence was evaluated under an applied field of 1000 Oe. The solid lines correspond to the best-fits to a generalized Debye model.

The resulting fit yields comparable values of U_{eff}/k_B = 34.27(1) K and τ_0 = 2.89(7) × 10^{-6} s (Figure 6).

$$\tau^{-1} = AH^2T + \tau_{QTM}^{-1} + \tau_0\exp(-U_{eff}/k_BT) \quad (3)$$

Before going through the dynamic magnetic properties of **Tb-tfac** and **Tb-hfac**, the field and temperature dependence of two maxima in χ''observed for **Tb-acac** should be commented as this phenomenon was clearly pronounced in **Tb-acac** compared to **Tb-tfac** and **Tb-hfac**. Similar kinds of field dependence of $\chi''$with two maxima have been observed before for other Ln-SMMs and might arise from intermolecular dipolar interactions between magnetic centres in a sample. [24, 67-71] In the low temperature regime, intermolecular dipolar interactions can generate a sufficiently wide dipolar field distribution in the sample which results in two distinct domains of the total magnetic field in which one relaxation process dominates the other (QTM vs. direct). [24, 68] The dominance of one relaxation process over the other can be controlled by the temperature and particularly by the applied dc field. Although the intermolecular dipolar couplings clearly influence almost as equally as intramolecular magnetic interactions to the magnetic properties of **Tb-acac** as mentioned above, it cannot be unambiguously concluded from their small values (Table S5) and the total sum of calculated intra- and intermolecular couplings ($J_{intra+inter\_dip}$ = 0.16 cm^{-1}) if the two observed maxima in χ''originate from the sufficiently wide dipolar field distribution within the sample. Moreover, in order to see two maxima in χ'', the ground (quasi)-doublet should be well separated from the first excited (quasi)-doublet otherwise the Orbach process may contribute to the formation or the destruction of the two maxima in conjunction with the QTM and direct process.[24, 68] Because the ground and first excited quasi-doublets are not separated by several hundred wavenumbers but only by 101 cm^{-1} in **Tb-acac** as shown by the *ab initio* calculations, we cannot completely rule out the involvement of the Orbach process to the presence of two maxima in χ'' at the low temperature regime where dynamic magnetic measurement were carried out. This assumption is in line with the fits performed for the high frequency region of the field and temperature dependent data that showed the contribution of the Orbach process to the relaxation of the magnetization in **Tb-acac**.

The effect of imparting electron withdrawing groups on the diketonate ligand is first investigated with the **Tb-tfac** complex. As can be seen in both field and temperature dependent χ''magnetic susceptibility plots (Figure S12), **Tb-tfac** exhibits a similar magnetic relaxation profile as **Tb-acac**. Indeed, two magnetic relaxations processes can be isolated, with the low frequency process appearing to be frequency independent. This again suggests the significant influence of a QTM mechanism. Unfortunately, the high frequency process, which may be thermally activated, as in **Tb-acac**, only displays tails of peaks within the instrument window. This precludes any meaningful analysis of the slow relaxation dynamics; however, it is clear that the addition of fluorine groups in the non-Kramers Tb^{3+} system is detrimental to the overall SMM behaviour. In **Tb-hfac**, which features even more electron-withdrawing fluorine atoms, only the low frequency process is visible under an applied field of 2000 Oe (Figure S13). Fitting of this data and extraction of the relaxation times confirms the prevalence of QTM (Table S9 and Figure S13). In all cases, even with the application of a static field, rapid relaxation through the ground state is central in the lack of a significant energy barrier. This becomes particularly evident in the ac magnetic susceptibility data of **Tb-tfac** and **Tb-hfac** wherein the contributions of QTM control the main magnetic relaxation pathways. Previous work on the effect of electron withdrawing groups on the slow magnetic relaxation dynamics of dinuclear systems have shown that two key factors must be considered.[16, 72] The first takes into account direct structural changes that would alter the ligand field of the Tb^{3+} ions and thus Tb-$O_{diketonate}$ and Tb-N_{bpm} distances need to be considered. At the same time, it is important to note that a change in the coordination environment of **Tb-hfac**, which is 9-coordinate, alter the crystal field splitting, as shown by calculations, and thus, the magnetic behaviour. As

10.1002/chem.201902837

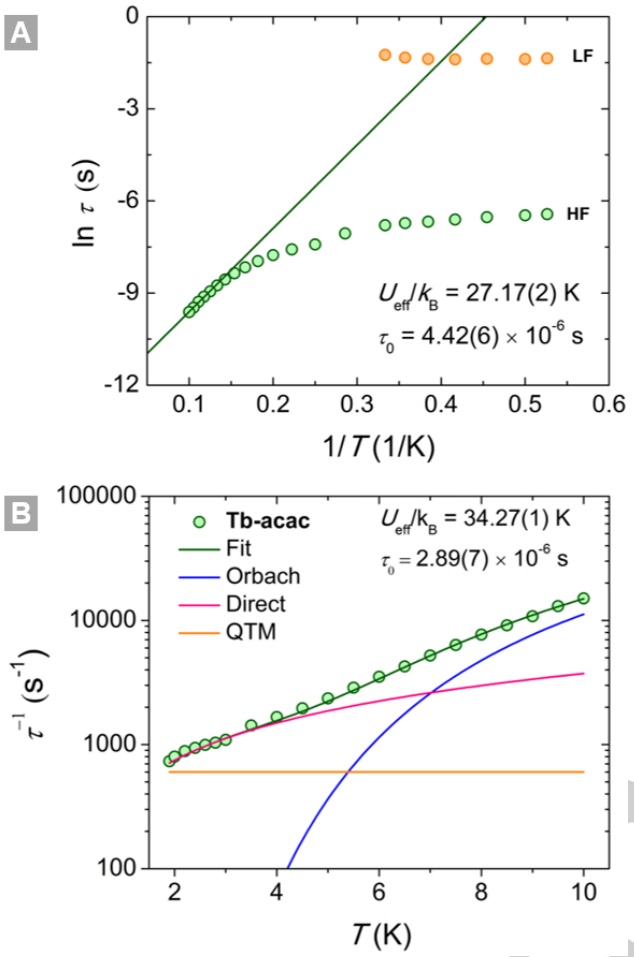

Figure 6. (A): Arrhenius plot of **Tb-acac** showing the magnetic relaxation time under a 1000 Oe applied field for the high (HF) and low frequency (LF) processes. The green line corresponds to the linear fit of the high temperature data. (B): Temperature dependence of the magnetization relaxation times. The solid line represents the best-fit using Equation (3) and takes into account Orbach, direct and QTM processes.

such, while we provide a detailed description of the ac magnetic susceptibility, care must be taken to avoid a direct comparison between eight- and nine-coordinate complexes. The addition of increasing amounts of fluorine atoms within the diketonate ligands leads to a decrease in the average Tb-N_{bpm} distances. This is highlighted by a comparison of the structures of **Tb-acac** and **Tb-tfac**, in which the average Tb-N_{bpm} distance decreases from 2.63 to 2.57 Å. Meanwhile, the average Tb-$O_{diketonate}$ distances remain relatively unchanged with an average value of 2.33 Å in both complexes. Interestingly, a major difference between the three complexes concerns the tunnel splitting. All exhibit tunnelling gaps in the ground pseudo doublet, which along with other magnetic properties resulting in the low symmetry coordination environments explain the poor SMM performance, however, the axiality and tunnelling gap are largest and second smallest, respectively, in **Tb-acac** leading to an improved slow relaxation of the magnetization (*vide infra*). Next, the change in the direction of the magnetic anisotropy, due to the addition of electron withdrawing groups, should be evaluated. The orientation of the main magnetic axis for all individual Tb^{3+} is depicted in Figure 7, and reveals that they are tilted away from the plane of the bridging bpm ligand. This indicates that the diketonate ligands generate a stronger crystal field compared to the neutral bpm ligand. Even though the orientation of the main magnetic axis is rather similar in all complexes, the axiality of **g**-tensor of ground quasi-doublets varies slightly due to the electron withdrawing groups (*vide infra*). It should also be noted that the presence of two crystallographically independent dinuclear complexes within **Tb-hfac** (referred to as **Tb-hfacA** and **Tb-hfacB**) can lead to slight changes in the orientation of the anisotropy axes and in the crystal field. Further discussion of the calculated magnetic anisotropy axes and **g**-tensors can be found below.

Ab-initio calculations

The standard CASSCF/SO-RASSI calculations followed by the SINGLE_ANISO routine were used to calculate the energy spectra and magnetic properties of **Tb-acac Tb-tfac**, **Tb-hfac**. (see computational details). In case of **Tb-hfac**, the calculations were carried out for both, **Tb-hfacA** and **Tb-hfacB**, crystallographic independent molecules.

The energy spectrum of **Tb-acac** and **Tb-tfac** are presented in Table S10 and S11, respectively. It is evident from these two Tables that the small structural changes associated with substituent change ($CH_3 \rightarrow CF_3$) do not only affect the positions of the energy levels but they also influence the tunnelling gaps of quasi-doublets: the energy levels of **Tb-acac** and **Tb-tfac** are rather similar up to the 6th spin-orbit states after which they start to deviate and **Tb-tfac** shows slightly larger tunnelling gaps than **Tb-acac** within the identified quasi-doublets (Tables S10 and S11). More dramatic changes are observed in the energy spectra of the investigated Tb_2 complexes when the coordination number around Tb^{3+} ions increases from eight to nine. The energy spectra of **Tb-hfacA** and **Tb-hfacB** arising from the ground atomic multiplet $^7F_6$ of Tb^{3+} ion are narrower compared to the energy

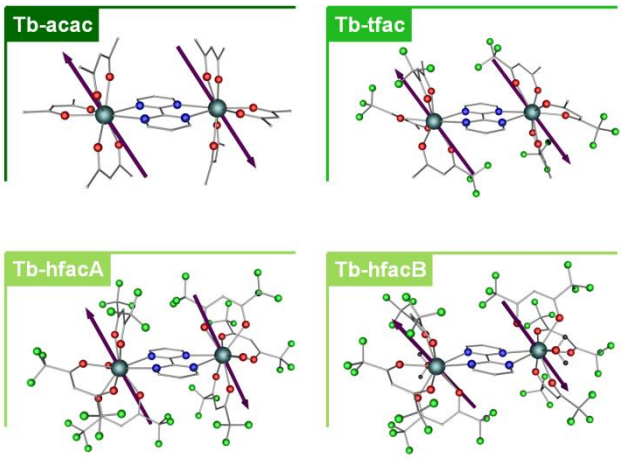

Figure 7. The orientation of the main magnetic axes of the ground quasi-doublets for the Tb_2 complexes.

spectra of **Tb-acac** and **Tb-tfac** (Tables S10-S13). The stabilization of the ground quasi-doublet is also larger for **Tb-acac** and **Tb-tfac** than for **Tb-hfacA** and **Tb-hfacB** as shown by the calculated energy gaps between the ground quasi doublets and first excited quasi-doublets (~100 cm^{-1} for **Tb-acac** and **Tb-tfac**; ~ 35 cm^{-1} for **Tb-hfacA** and **Tb-hfacB**). Similar results have been also reported for tetrathiafulvalene-fused dipyridophenazine based Kramers Dy^{3+} systems in which the addition of fluorine groups to the backbone of coordinating acac ligands not only increased the efficiency of QTM but also lead to the narrower energy spectrum of ground multiplet like in investigated Tb^{3+} systems.[73]

Interestingly, the main magnetic axis of the ground quasi-doublet of all individual Tb^{3+} ions is similarly tilted away from the plane of the bridging bpm ligand as depicted in Figure 7. This indicates that the diketonate ligands generate a stronger crystal ligand field compared to the neutral bpm ligand as mentioned above. The closer inspection of the **g**-tensors of the ground quasi-doublets reveal that all investigated Tb-complexes deviate slightly from the ideal highly symmetrical axial system: the g_z values for **Tb-acac**, **Tb-tfac**, **Tb-hfacA**, and **Tb-hfacB** are 17.83, 17.56, 16.98 and 17.59, respectively. Thus, they are 0.2–1.0 smaller than the ideal g_z value of 18.00 for the perfect axial ground doublet of $M_J = \pm 6$ state.[74] Based on the g_z values of the ground quasi-doublets of all studied system, it can be concluded that the most axial complex is **Tb-acac**. The result can be rationalized by magneto-structural correlations. Firstly, the addition of increasing amounts of fluorine atoms within the diketonate ligands leads to a decrease in the average Tb-N_{bpm} distances. This is highlighted by a comparison of the structures of **Tb-acac** and **Tb-tfac**, in which the average Tb-N_{bpm} distance decreases from 2.63 Å to 2.57 Å. The shortening of Tb-N_{bpm} bond generates a stronger equatorial ligand field around Tb^{3+} ions that results in a less axial system as exemplified the g_z values of the ground quasi-doublets of **Tb-acac** and **Tb-tfac** (17.83 vs. 17.56). Meanwhile, the average Tb-$O_{diketonate}$ distances remain relatively unchanged with an average value of 2.33 Å in both complexes. Secondly, the change of the coordination number from eight to nine decreases also the axiality as illustrated with **g**-tensors of **Tb-acac**, **Tb-hfacA**, and **Tb-hfacB**. Although **Tb-acac** is the most axial systems, significant angles between the main magnetic axes of ground and excited quasi-doublets underpin the fact that all Tb^{3+} ions in **Tb-acac**, **Tb-tfac**, **Tb-hfacA** and **Tb-hfacB** reside in rather low symmetry coordination environments (Tables S10-S13). This result is fully in line with the *R* values obtained from the luminescence measurements.

The investigation of the percentage decomposition of the SO-RASSI wavefunctions of the ground quasi-doublets reveals that in all complexes, the ground state quasi-doublet is composed of equal mixture of the $M_J = +6$ and $M_J = -6$ states with small contributions arising from excited spin-orbit states (Tables S14-S17). The mixing of the ground quasi-doublets by the excited spin-orbit states is stronger in nine-coordinated complexes, particularly in **Tb-hfacA**, than in eight-coordinated complexes. The decomposition of the excited spin-orbit states is also altered when the electron withdrawing groups are introduced into the diketonate framework and/or coordination number is changed from eight to nine. Most importantly, all excited quasi-doublets and non-degenerated spin-orbit states show considerable mixing between states, thus, they cannot be unambiguously defined to any pure M_J state.

The qualitative energy barriers of Tb_2 complexes were investigated by using the previously reported approach.[75] As seen from Figure 8, all complexes display rather high tunnelling gaps within the ground quasi-doublet that is typical for non-Kramers ion. This readily explains along with the direct mixing of ground quasi-doublets why **Tb-acac**, **Tb-tfac**, **Tb-hfacA**, and **Tb-hfacB** do not show the slow relaxation of the magnetization without the applied dc field. In the absence of the applied dc field, the slow relaxation of the magnetization of non-Kramers ion within low symmetry coordination environment readily occurs through the quantum tunnelling of magnetization (QTM) within the ground quasi-doublet.[18, 76-78] However, the direct mixing between the spin-orbit states during ac measurements can be decreased by applying the optimal dc field that lowers the rate of the QTM. Thus, the most axial system of the studied complexes, **Tb-acac**, displays slow relaxation of the magnetization when an optimal dc field of 1000 Oe is used during the ac measurements. For **Tb-acac**, the calculated energy barrier for the Orbach process is higher than the experimentally determined energy barrier suggesting that QTM and direct relaxation process contributes more than Orbach process to the slow relaxation of magnetization within **Tb-acac**. It should be stressed here that observed changes in the **g**-tensors, tunnelling gaps, and decomposition of the SO-RASSI wavefunctions of **Tb-acac**, **Tb-tfac**, **Tb-hfacA**, and **Tb-hfacB** are moderate or small when the CH_3 group is substituted by the CF_3 group and/or the coordination number is increased from eight to nine, but still they influence the magnetic properties of the investigated system as illustrated by the experimental SQUID measurements.

Conclusions

The use of different diketonates for the preparation of a family of Tb_2 complexes has impacted both the optical and magnetic properties of said compounds. Importantly, while we show that increasing the number of fluorine atoms within the ligand framework can induce a change in the physical properties, these features depend on two drastically different aspects. On one side, the position of the triplet state of the ligands (diketonate and bpm) – and specifically the intersection of the energy wells of the electronic levels involved in the photoluminescence – is a key factor. This affects the photoluminescence efficiency and the performance of the complexes as luminescent thermometers, both in terms of working temperature range and relative thermal sensitivity. On the other hand, although partially influencing also the emission intensity, the coordination environment and the crystal ligand field are crucial in dictating the magnetic behaviour, and thus the SMM performance. Being these two properties closely intertwined, our findings point to a design of multifunctional lanthanide complexes based on a case-by-case fine-tuning of the ligand scaffold. This is achieved through slight modifications that depend on the lanthanide ion of choice and the properties sought

10.1002/chem.201902837

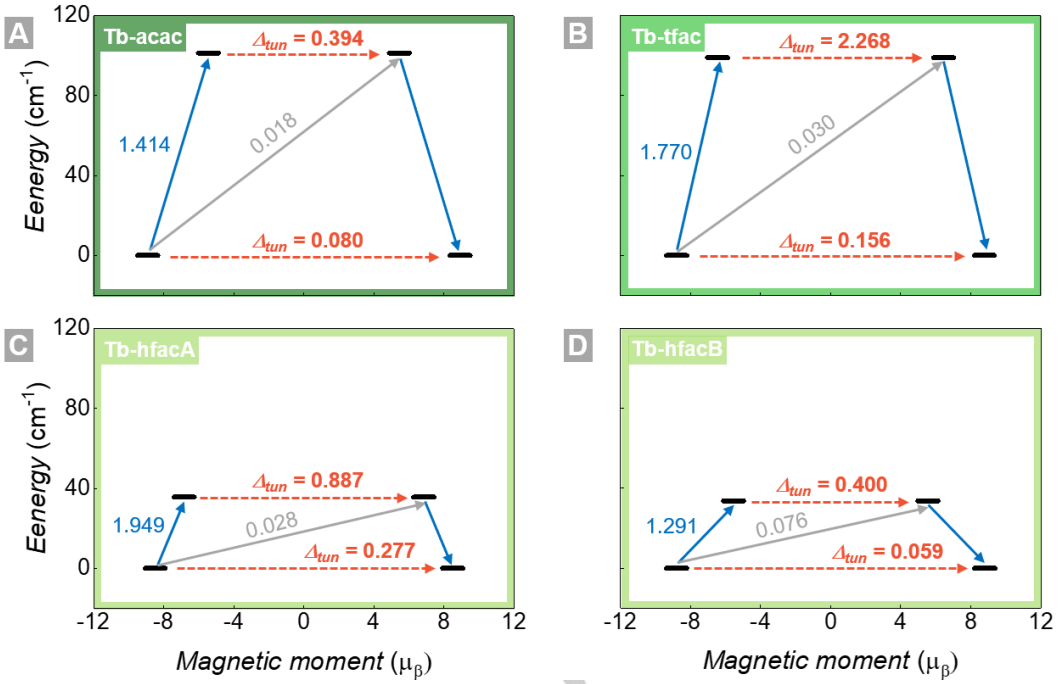

Figure 8. Qualitative relaxation barrier for **Tb-acac** (A), **Tb-tfac** (B), **Tb-hfacA** (C), and **Tb-hfacB** (D). The numbers show the transition probabilities (μ_B) or tunnelling gaps (Δ_{tun} [cm^{-1}]) between quasi-doublets. Blue and grey solid arrows show the transition probabilities for the direct vertical transitions and Orbach process, respectively, whereas red dashed arrows represent tunnelling gaps between quasi degenerated doublets.

after. To that end, the properties imparted by electron donating or withdrawing groups have seldom been investigated from the standpoint of the luminescence thermometry. This is in stark contrast to molecular magnetism, wherein small changes to the molecular structure are exceedingly probed in a systematic fashion. As such, in this study, we highlight the different factors (*i.e.*, triplet state energy of the ligands and coordination environment of the metal) that should be considered when simultaneously combining magnetism and luminescence within a discrete molecule.

Experimental Section

Experimental Details. Chemicals

All chemicals were purchased from Alfa Aesar, STREM Chemicals, Ark Pharm, and Sigma Aldrich and were used as received without further purification.

Synthesis

The ligand 2,2'-bipyrimidine (bpm) was prepared as per established synthetic method described elsewhere,[79] while the complexes were synthesized following previously reported procedures[41, 42] as briefly outlined below.

[Tb_2(bpm)(acac)$_6$] (Tb-acac). A bpm solution (39.54 mg, 0.25 mmol) in acetonitrile (1.5 mL) was added to a 5 mL stirring slurry of Tb(acac)$_3$·3H_2O (99.9%, 228.1 mg, 0.50 mmol). The resulting mixture was heated to 60 °C and refluxed for 2 h, during which time it turned clear. Afterwards the solution was filtered, allowed to cool to room temperature and then transferred to a fridge. The product was recovered as yellow crystals. (Yield ~82%) Elemental Analysis: Calcd.: C, 42.63%; H, 4.52%; N, 5.23%; Exp.: C, 42.22%; H, 4.76%; N, 5.14%.

[Tb_2(bpm)(tfac)$_6$] (Tb-tfac). A saturated ammonia solution (1.2 mL, 1.62 mmol) was added to a stirring solution of 1,1,1-trifluoroacetylacetone (197 µL, 1.62 mmol) in 5 mL of ethanol. The resulting mixture was allowed to stir for 15 min after which a 5 mL ethanol solution of bpm (42.7 mg, 0.27 mmol) followed by $TbCl_3$·6H_2O (99.9%, 202 mg, 0.54 mmol) was swiftly added. The resulting mixture was allowed to stir for 1 h after which the solution was filtered and allowed to evaporate in open air. The resulting solid was washed with a small amount of chloroform and the crude product suspended in 15 mL of dichloromethane and stirred for 30 min. The resulting solution was allowed to evaporate slowly to yield the product as clear, colourless crystals. (Yield ~79%) Elemental Analysis: Calcd.: C, 32.74%; H, 2.17%; N, 4.02%; Exp.: C, 33.01%; H, 2.08%; N, 4.13%.

[Tb_2(bpm)(hfac)$_6$(H_2O)$_2$] (Tb-hfac). This complex was synthesized following the same procedure reported above for Tb-tfac with the only difference that 1,1,1,5,5,5-hexafluoroacetylacetone (227 µL, 1.62 mmol) was used instead of 1,1,1-trifluoroacetylacetonate. (Yield ~75%) Elemental Analysis: Calcd.: C, 26.01%; H, 0.92%; N, 3.19%; Exp.: C, 25.73%; H, 1.31%; N, 3.29%.

Characterization methods

Infrared (IR) spectra were obtained on a Nicolet Nexus 550 FT-IR spectrometer equipped with an ATR using transmission mode in the 4000-600 cm^{-1} range. Thermogravimetric analysis (TGA) measurements were carried out on a SDT Q600 (TA Instruments) with a constant heating rate of 10 K/min and a synthetic air flow of 10 L/h using 2-3 mg of sample in a platinum pan. Crystallographic data were collected on a Bruker AXS SMART or KAPPA single-crystal diffractometer equipped with a sealed Mo

tube source (λ = 0.71073 Å) and APEX II CCD detector. The crystals were mounted on a thin glass fibre, affixed using paraffin oil and cooled to 200.15 K. The data reduction included multi-scan absorption correction (SADABS). Raw data collection and processing were performed with APEX II software package from BRUKER AXS.[80]. The crystal structures were solved and refined using the SHELXTL program suite (v. 2012, A. S. S.; Bruker AXS: Madison, W., 2005). Direct methods were used yielding all non-hydrogen atoms, which were refined with anisotropic thermal parameters. All hydrogen atom positions were calculated based on the geometry of their respective atoms.

Photoluminescence data were obtained on a Fluorolog-3 spectrofluorometer (Horiba FL3-22-iHR320), with double-gratings (1200 g/mm, 330 nm blaze) in the excitation monochromator and double-gratings (1200 g/mm, 500 nm blaze) in the emission monochromator. An ozone-free Xenon lamp of 450 W (Ushio) was used as a radiation source. The excitation spectra were corrected in real time according to the lamp intensity and the optical system of the excitation monochromator using a silicon diode as a reference. The emission spectra were recorded using the front face mode at 22.51° and corrected according to the optical system of the emission monochromator and the photomultiplier response (Hamamatsu R928P). The emission decay curves were obtained with a flash 150 W Xenon lamp using a time-correlated single photon counting (TCSPC) system. The absolute quantum yields were measured using a Quanta-φ (Horiba F-309) integrating sphere equipped with an optical-fibres bundle (NA=0.22-Horiba-FL-3000/FM4-3000) using ligand-centred excitations. The integrated sphere was calibrated using sodium salicylate as a standard. For liquid-N_2-to-room-temperature thermometry, the measurements were performed using a cryostat (Janis Research Company CCS-450), controlled by a Lakeshore 335 temperature controller. The temperature was lowered to 77 K and increased stepwise to 300 K. For each step, upon reaching the target temperature, 10 min were waited to guarantee thermal stabilization. For high-temperature thermometry, the sample was placed in a platinum crucible inside a Linkam TS1500 stage coupled with a Linkam T95-HT controller. The accessory was coupled *via* optical fibre to a Fluorolog-3 spectrofluorometer (Horiba FL3-22-iHR320) as reported above. An ozone-free Xenon lamp of 450 W (Ushio) was used as a radiation source. The temperature was increased stepwise from 298 to 398 K. For each step, upon reaching the target temperature, 10 min were waited to guarantee thermal stabilization. All the photoluminescence measurements were performed in solid-state.

Magnetic susceptibility measurements were performed on a Quantum Design SQUID magnetometer MPMS-XL7, operating between 1.9 and 300 K and applied fields of up to 7 T. Direct current (dc) susceptibility measurements were performed on finely ground polycrystalline samples (17.7, 11.4 and 7.2 mg, for **Tb-acac**, **Tb-tfac** and **Tb-hfac** respectively) restrained in a matrix of vacuum grease and wrapped in a polyethylene membrane. Alternating current (ac) susceptibility measurements were performed under an oscillating ac field of 3.78 Oe and ac frequencies ranging from 0.1 to 1488 Hz. Magnetization *vs.* field measurements were collected at 100 K to check for the presence of ferromagnetic impurities, which were found to be absent in all samples. Diamagnetic corrections were applied for the sample holder and the inherent diamagnetism of the prepared sample was estimated with the use of Pascal's constants.

Computational details

The geometries of **Tb-acac**, **Tb-tfac**, **Tb-hfacA**, and **Tb-hfacB** were taken from the crystal structures. **Tb-hfacA** and **Tb-hfacB** refer to the two distinct dimers in the unit cell of **Tb-hfac**. Prior to the standard CASSCF/SO-RASSI calculations (see below),[81, 82] the positions of hydrogen atoms were optimized at the RI-PBE-D3/def2-TZVP level of theory,[83-91] and the positions of all other atoms were kept frozen. In optimizations, Tb^{3+} ions were replaced with Y^{3+} to avoid convergence problems and the core electrons of Y^{3+} ions were treated with the effective core potential.[92] The RI approximation was used to the speed up all RI-PBE-D3/def2-TZVP calculations,[85-87] whereas dispersion forces were taken into account using the dispersion correction in conjunction with the damping function.[90, 91] All RI-PBE-D3/def2-TZVP calculations were carried out by Turbomole program package.[93]

In order to get more insight into the magnetic properties of **Tb-acac**, **Tb-tfac**, **Tb-hfacA**, and **Tb-hfacB**, the standard CASSCF/SO-RASSI[76, 79] calculations followed by the SINGLE_ANISO[75, 94, 95] routine as implemented in the Molcas quantum chemistry program package version 8.2[96] were performed for them. Because all investigated complexes display inversion symmetry, the CASSCF/SO-RASSI calculations were done only for one Tb^{3+} centre while other was replaced with Y^{3+} ion. In the CASSCF/SO-RASSI calculations, the ANO-RCC-VTZP and ANO-RCC-VDZP basis sets were used for Tb^{3+} and all other atoms (H, C, N, O, F, Y), respectively.[97, 98] The scalar relativistic effects were taken into account using the exact two component (X2C) transformation.[99-101] The Cholesky decomposition with the threshold value of 10^{-8} was employed in two electron integrals calculations. For Tb^{3+} ion, the active space of eight electrons and seven 4f-orbitals would generate 7 septet, 140 quintet, 588 triplet, and 490 singlet spin states, however, only 7 septet and 140 quintet states were solved in the SA-CASSCF calculations and mixed by the spin-orbit coupling in the subsequent SO-RASSI calculations. For all investigated complexes, the local magnetic properties (*g* tensors, transition magnetic moments, and orientation of magnetic axis) were extracted from the SO-RASSI wave functions using the SINGLE_ANISO routine. The intramolecular exchange coupling constant ($J_{ij}^{Lines\_exh}$) between Tb^{3+} ions were determined using the Lines model[102] as implemented in the POLY_ANISO[103, 104] program and by fitting the calculated χT and *M* to experimental data by varying the exchange coupling constant with small increments of 0.001 cm^{-1}. Two lowest lying spin-orbit functions were included from both centres to the exchange coupling, and dipolar coupling was taken also into account during the fitting procedure. By assuming that the local magnetic anisotropy of each Tb^{3+} ions are of the Ising type ($g_x = g_y = 0$ and $g_z \sim 18$), the obtained Lines exchange coupling constants can be converted to the Ising exchange parameters using Equation 4:

$$\tilde{J}_{ij}^{Ising\_exh} = 36 J_{ij}^{Lines\_exh} cos\varphi_{ij} \quad (4)$$

where φ_{ij} is the angle between the main anisotropy axes of the interacting sites.[105] The Ising approximation holds reasonably well for **Tb-acac**, **Tb-tfac** and **Tb-hfacB** as their g_z values of the ground quasi-doublet are larger than 17.5 and $g_x = g_y = 0$. The total intramolecular magnetic interaction was calculated by using the following Hamiltonian:

$$\tilde{H} = -(\tilde{J}_{ij}^{Ising\_exh} + \tilde{J}_{ij}^{Ising\_dip})\tilde{S}_{iz}\tilde{S}_{jz} \quad (5)$$

in which $\tilde{S}_{iz}$ and $\tilde{J}_{ij}^{Ising\_dip}$ are the projection of the pseudo-spin on the anisotropy axis of site *i* and dipolar coupling constant, respectively, of which the latter one can be calculated using the expression (Eq. 6):[105]

$$\tilde{J}_{ij}^{Ising\_dip} = \mu_B^2 g_{zi} g_{zj} \frac{cos\theta_{ij} - 3cos\theta_{in} cos\theta_{jn}}{r^3}. \quad (6)$$

In Equation 6 μ_B is the Bohr magneton, g_{zi} is the component of **g**-tensor of the *i*th centre along the z direction, θ_{ij} is the angle between the anisotropy axes of the *i*th and *j*th centres, θ_{in} is the angle between the principal anisotropy axis of *i*th centre and the vector connecting two Tb^{3+} ions and r is the distance between two Tb^{3+} ions. Equation 3 was also used to calculate intermolecular dipolar constants between neighbouring Tb^{3+} ions in **Tb-acac**. The intermolecular dipolar coupling constants were calculated for all Tb^{3+} ion pairs that resided within 15 Å from "central" Tb^{3+} ion. Moreover, when calculating intermolecular dipolar coupling constants, it was assumed that the main magnetic axis of each Tb^{3+} ion in the crystal structure of **Tb-acac** has the same orientation because **Tb-acac** crystallizes in $P\bar{1}$ space group in which only symmetry operation, in

addition to identity, is inversion. For the sake of the clarity we use the following notation in the text: $J_{ij}^{Ising\_exh} = J_{intra\_exh}$ and $J_{ij}^{Ising\_dip} = J_{intra\_dip} = J_{inter\_dip}$.

It should be also mentioned that the calculated plots of χT and *M* for **Tb-acac**, **Tb-tfac**, and **Tb-hfac** were scaled 5%, 1.5%, and 3.0% to obtain a better fit with the experimental data. Additionally, the calculated plot of *M* for Tb-acac was scaled 5%. Discrepancies between experimental and calculated data most likely arises from the exclusion of dynamic electron correlating effects in the CASSCF calculations, that is, the electron correlation outside of the 4f orbital space has been neglected in calculations. It has been shown that the electron correlation outside of 4f orbital space affects the crystal-field splitting of ground multiplet of lanthanide ions that further influences the rate of thermal depopulation of excited levels when the temperature is decreased.[95] Also, the degree of mixing of states will be altered by the crystal field splitting because of the Zeeman interaction.

Acknowledgements

M.M. and E.H. thank the University of Ottawa, the CFI and NSERC for their financial support. F.A.S. and D.A.G. are indebted to CNPq, CAPES and FAPESP (grant: 2013/22127-2) and INOMAT (FAPESP grant: 2014/50906-9), for financial support. Authors would like to thank the Multiuser Laboratory of Advanced Optical Spectroscopy – Institute of Chemistry – UNICAMP. J.O.M. acknowledges the Academy of Finland for the funding (315829, 320015) as well as Prof. H. M. Tuononen, University of Jyväskylä, Jyväskylä, Finland for providing computational resources.

Keywords: lanthanide complexes • photoluminescence • luminescence thermometry • single-molecule magnets • opto-magnetic

Crystallographic information for the complex **Tb-hfac** can be found at Cambridge Crystallographic Data Centre CCDC (https://www.ccdc.cam.ac.uk/), entry # 1904524.

[1] Y. Che, A. Datar, X. Yang, T. Naddo, J. Zhao, L. Zang, *J. Am. Chem. Soc.* **2007**, *129*, 6354-6355.
[2] N. A. Zaidi, J. P. Foreman, G. Tzamalis, S. C. Monkman, A. P. Monkman, *Adv. Funct. Mater.* **2004**, *14*, 479-486.
[3] A. C. Aragones, N. Darwish, J. Im, B. Lim, J. Choi, S. Koo, I. Diez-Perez, *Chem. Eur. J.* **2015**, *21*, 7716-7720.
[4] M. Lanznaster, A. Neves, A. J. Bortoluzzi, A. M. Assumpcao, I. Vencato, S. P. Machado, S. M. Drechsel, *Inorg. Chem.* **2006**, *45*, 1005-1011.
[5] H. Neuvonen, K. Neuvonen, A. Koch, E. Kleinpeter, P. Pasanen, *J. Org. Chem.* **2002**, *67*, 6995-7003.
[6] C. Popeney, Z. Guan, *Organometallics* **2005**, *24*, 1145-1155.
[7] S. F. Ni, L. Dang, *Phys. Chem. Chem. Phys.* **2016**, *18*, 4860-4870.
[8] J. Yuan, J. Zhao, F. Song, W. Xu, Y. Mu, J. Chen, Z. Zhang, *Appl. Organomet. Chem.* **2014**, *28*, 484-494.
[9] S. Abou-Hatab, V. A. Spata, S. Matsika, *J. Phys. Chem. A* **2017**, *121*, 1213-1222.
[10] M. M. Duvenhage, H. G. Visser, O. M. Ntwaeaborwa, H. C. Swart, *Physica B Cond. Matter* **2014**, *439*, 46-49.
[11] B. Gao, L. Chen, T. Chen, *Phys. Chem. Chem. Phys.* **2015**, *17*, 25322-25332.
[12] S. Sivakumar, M. L. Reddy, A. H. Cowley, K. V. Vasudevan, *Dalton Trans.* **2010**, *39*, 776-786.
[13] H. Xu, R. Chen, Q. Sun, W. Lai, Q. Su, W. Huang, X. Liu, *Chem. Soc. Rev.* **2014**, *43*, 3259-3302.
[14] J.-C. G. Bünzli, *Coord. Chem. Rev.* **2015**, *293-294*, 19-47.
[15] L. Armelao, S. Quici, F. Barigelletti, G. Accorsi, G. Bottaro, M. Cavazzini, E. Tondello, *Coord. Chem. Rev.* **2010**, *254*, 487-505.
[16] F. Habib, G. Brunet, V. Vieru, I. Korobkov, L. F. Chibotaru, M. Murugesu, *J. Am. Chem. Soc.* **2013**, *135*, 13242-13245.
[17] D. N. Woodruff, R. E. Winpenny, R. A. Layfield, *Chem. Rev.* **2013**, *113*, 5110-5148.
[18] J. L. Liu, Y. C. Chen, M. L. Tong, *Chem. Soc. Rev.* **2018**, *47*, 2431-2453.
[19] K. R. Vignesh, S. K. Langley, K. S. Murray, G. Rajaraman, *Inorg. Chem.* **2017**, *56*, 2518-2532.
[20] S. Thiele, F. Balestro, R. Ballou, S. Klyatskaya, M. Ruben, W. Wernsdorfer, *Science* **2014**, *344*, 1135-1138.
[21] M. Lopes, A. Candini, M. Urdampilleta, A. Reserbat-Plantey, V. Bellini, S. Klyatskaya, L. Marty, M. Ruben, M. Affronte, W. Wernsdorfer, N. Bendiab, *ACS Nano* **2010**, *4*, 7531-7537.
[22] G. Cucinotta, L. Poggini, A. Pedrini, F. Bertani, N. Cristiani, M. Torelli, P. Graziosi, I. Cimatti, B. Cortigiani, E. Otero, P. Ohresser, P. Sainctavit, A. Dediu, E. Dalcanale, R. Sessoli, M. Mannini, *Adv. Funct. Mater.* **2017**, *27*, 1703600.
[23] M. Mannini, F. Bertani, C. Tudisco, L. Malavolti, L. Poggini, K. Misztal, D. Menozzi, A. Motta, E. Otero, P. Ohresser, P. Sainctavit, G. G. Condorelli, E. Dalcanale, R. Sessoli, *Nat. Commun.* **2014**, *5*, 4582.
[24] J. D. Rinehart, M. Fang, W. J. Evans, J. R. Long, *J. Am. Chem. Soc.* **2011**, *133*, 14236-14239.
[25] A. T. Bui, A. Grichine, A. Duperray, P. Lidon, F. Riobe, C. Andraud, O. Maury, *J. Am. Chem. Soc.* **2017**, *139*, 7693-7696.
[26] D. Errulat, B. Gabidullin, M. Murugesu, E. Hemmer, *Chem. Eur. J.* **2018**.
[27] N. Hildebrandt, K. D. Wegner, W. R. Algar, *Coord. Chem. Rev.* **2014**, *273-274*, 125-138.
[28] Y. W. Wang, S. B. Liu, Y. L. Yang, P. Z. Wang, A. J. Zhang, Y. Peng, *ACS Appl. Mater. Interfaces* **2015**, *7*, 4415-4422.
[29] K. Binnemans, *Chem. Rev.* **2009**, *109*, 4283-4374.
[30] O. Kotova, S. Comby, C. Lincheneau, T. Gunnlaugsson, *Chem. Sci.* **2017**, *8*, 3419-3426.
[31] L. D. Carlos, R. A. Ferreira, Z. Bermudez Vde, S. J. Ribeiro, *Adv. Mater.* **2009**, *21*, 509-534.
[32] J. Rocha, C. D. S. Brites, L. D. Carlos, Chem. Eur. J. **2016**, 22, 14782-14795.
[33] S. Katagiri, Y. Tsukahara, Y. Hasegawa, Y. Wada, *Bull. Chem. Soc. Jap.* **2007**, *80*, 1492-1503.
[34] D. A. Gálico, I. O. Mazali, F. A. Sigoli, *J. Lumin.* **2017**, *192*, 224-230.
[35] J. Yu, L. Sun, H. Peng, M. I. J. Stich, *J. Mater. Chem.* **2010**, *20*, 975-981.
[36] S. M. Bruno, D. Ananias, F. A. Paz, M. Pillinger, A. A. Valente, L. D. Carlos, I. S. Goncalves, *Dalton Trans.* **2015**, *44*, 488-492.
[37] D. A. Gálico, Í. O. Mazali, F. A. Sigoli, *New J. Chem.* **2018**, *42*, 18541-18549.
[38] D. V. Lapaev, V. G. Nikiforov, V. S. Lobkov, A. A. Knyazev, Y. G. Galyametdinov, *J. Mater. Chem. C* **2018**, *6*, 9475-9481.
[39] D. Errulat, R. Marin, D. A. Gálico, K. L. M. Harriman, A. Pialat, B. Gabidullin, F. Iikawa, O. D. D. Couto Jr, J. O. Moilanen, E. Hemmer, F. A. Sigoli, M. Murugesu, *ACS Cent. Sci.* **2019**, DOI: 10.1021/acscentsci.9b00288
[40] G. Brunet, R. Marin, M.-J. Monks, U. Resch-Genger, D. A. Gálico, F. A. Sigoli, E. A. Suturina, E. Hemmer, M. Murugesu, *Chem. Sci.* **2019**, DOI: 10.1039/C9SC00343F
[41] R. Ilmi, K. Iftikhar, *Polyhedron* **2015**, *102*, 16-26.
[42] G. Zucchi, T. Jeon, D. Tondelier, D. Aldakov, P. Thuéry, M. Ephritikhine, B. Geffroy, *J. Mater. Chem.* **2010**, *20*, 2114-2120.
[43] K. A. Romanova, A. Y. Freidzon, A. A. Bagaturyants, Y. G. Galyametdinov, *J. Phys. Chem. A* **2014**, *118*, 11244-11252.
[44] Z. Ahmed, K. Iftikhar, *Inorganica Chim. Acta* **2012**, *392*, 165-176.
[45] B. R. Judd, *Phys. Rev.* **1962**, *127*, 750-761.

[46] C. C. A. Görller-Walrand Gorllerwalrand, K. Binnemans, *Handbook of the Physics and Chemistry of Rare Earths*, **1996**, *23*, 121-283.
[47] L. Marciniak, K. Trejgis, *J. Mater. Chem. C* **2018**, *6*, 7092-7100.
[48] S. Freddi, L. Sironi, R. D'Antuono, D. Morone, A. Dona, E. Cabrini, L. D'Alfonso, M. Collini, P. Pallavicini, G. Baldi, D. Maggioni, G. Chirico, *Nano Lett.* **2013**, *13*, 2004-2010.
[49] C. D. S. Brites, S. Balabhadra, L. D. Carlos, Adv. Opt. Mater. **2018**, 7, 1801239.
[50] L. Labrador-Paez, M. Pedroni, A. Speghini, J. Garcia-Sole, P. Haro-Gonzalez, D. Jaque, *Nanoscale* **2018**, *10*, 22319-22328.
[51] N. F. Mott *Proceedings of the Royal Society of London. Series A. Mathematical and Physical Sciences* **1938**, *167*, 384-391.
[52] F. Seitz, *Transactions of the Faraday Society* **1939**, *35*, 74-85.
[53] Y. An, G. E. Schramm, M. T. Berry, *J. Lumin.* **2002**, *97*, 7-12.
[54] M. T. Berry, P. S. May, H. Xu, *J. Phys. Chem.* **1996**, *100*, 9216-9222.
[55] C. D. S. Brites, A. Millán, L. D. Carlos, in *Including Actinides*, **2016**, pp. 339-427.
[56] C. D. S. Brites, S. Balabhadra, L. D. Carlos, *Adv. Opt. Mater.* **2018**, *7*, 1801239.
[57] G. Brunet, M. Hamwi, M. A. Lemes, B. Gabidullin, M. Murugesu, *Commun. Chem.* **2018**, *1*, 88.
[58] K. Katoh, B. K. Breedlove, M. Yamashita, *Chem. Sci.* **2016**, *7*, 4329-4340.
[59] Y. Chen, C. Liu, F. Ma, D. Qi, Q. Liu, H. L. Sun, J. Jiang, *Chem. Eur J.* **2018**, *24*, 8066-8070.
[60] S.-D. Jiang, B.-W. Wang, G. Su, Z.-M. Wang, S. Gao, *Angew. Chem. Int. Ed.* **2010**, *122*, 7610-7613.
[61] K. Prša, J. Nehrkorn, J. Corbey, W. Evans, S. Demir, J. Long, T. Guidi, O. Waldmann, *Magnetochemistry* **2016**, *2*, 45.
[62] J. Miklovic, D. Valigura, R. Boca, J. Titis, *Dalton Trans.* **2015**, *44*, 12484-12487.
[63] S. Hazra, J. Titis, D. Valigura, R. Boca, S. Mohanta, *Dalton Trans.* **2016**, *45*, 7510-7520.
[64] E. Mamontova, J. Long, R. Ferreira, A. Botas, D. Luneau, Y. Guari, L. Carlos, J. Larionova, *Magnetochemistry* **2016**, *2*, 41.
[65] S. T. Liddle, J. van Slageren, *Chem. Soc. Rev.* **2015**, *44*, 6655-6669.
[66] R. J. Blagg, L. Ungur, F. Tuna, J. Speak, P. Comar, D. Collison, W. Wernsdorfer, E. J. McInnes, L. F. Chibotaru, R. E. Winpenny, *Nat. Chem.* **2013**, *5*, 673-678.
[67] S. K. Langley, N. F. Chilton, B. Moubaraki, K. S. Murray, *Inorg. Chem.* **2013**, *52*, 7183-7192.
[68] L. T. A. Ho, L. F. Chibotaru, *Phys. Rev. B* **2018**, *98*, 174418.
[69] E. Lucaccini, M. Briganti, M. Perfetti, L. Vendier, J.-P. Costes, F. Totti, R. Sessoli, L. Sorace, *Chem. - A Eur. J.* **2016**, *22*, 5552–5562.
[70] G. Peng, Y.-Y. Zhang, Z.-Y. Li, *Inorg. Chem. Commun*. **2017**, *77*, 40–43.
[71] M. Jeletic, P.-H. Lin, J. J. Le Roy, I. Korobkov, S. I. Gorelsky, M. Murugesu, *J. Am. Chem. Soc*. **2011**, *133*, 19286–19289.
[72] S. K. Langley, D. P. Wielechowski, B. Moubaraki, K. S. Murray, *Chem. Commun. (Camb.)* **2016**, *52*, 10976-10979.
[73] F. Pointillart, J. Jung, R. Berraud-Pache, B. Le Guennic, V. Dorcet, S. Golhen, O. Cador, O. Maury, Y. Guyot, S. Decurtins, et al., *Inorg. Chem*. **2015**, *54*, 5384–5397.
[74] L. Ungur, L. F. Chibotaru, *Phys. Chem. Chem. Phys.* **2011**, *13*, 20086-20090.
[75] L. Ungur, M. Thewissen, J. P. Costes, W. Wernsdorfer, L. F. Chibotaru, *Inorg. Chem.* **2013**, *52*, 6328-6337.
[76] C. A. P. Goodwin, D. Reta, F. Ortu, J. Liu, N. F. Chilton, D. P. Mills, *Chem. Commun. (Camb.)* **2018**, *54*, 9182-9185.
[77] S. K. Gupta, R. Murugavel, *Chem. Commun. (Camb.)* **2018**, *54*, 3685-3696.
[78] Y. S. Meng, S. D. Jiang, B. W. Wang, S. Gao, *Acc. Chem. Res.* **2016**, *49*, 2381-2389.
[79] P. F. H. Schwab, F. Fleischer, J. Michl, *J. Org. Chem.* **2002**, *67*, 443-449.
[80] G. M. Sheldrick, *Acta Crystallogr. A* **2008**, *64*, 112-122.
[81] B. O. Roos, R. Lindh, P. Å. Malmqvist, V. Veryazov, P.-O. Widmark, *Multiconfigurational Quantum Chemistry*, **2016**.
[82] P. Å. Malmqvist, B. O. Roos, B. Schimmelpfennig, *Chem. Phys. Lett.* **2002**, *357*, 230-240.
[83] J. P. Perdew, K. Burke, M. Ernzerhof, *Phys. Rev. Lett.* **1996**, *77*, 3865-3868.
[84] J. P. Perdew, Y. Wang, *Phys. Rev. B* **1992**, *45*, 13244-13249.
[85] K. Eichkorn, O. Treutler, H. Öhm, M. Häser, R. Ahlrichs, *Chem. Phys. Lett.* **1995**, *240*, 283-290.
[86] K. Eichkorn, O. Treutler, H. Öhm, M. Häser, R. Ahlrichs, *Chem. Phys. Lett.* **1995**, *242*, 652-660.
[87] K. Eichkorn, F. Weigend, O. Treutler, R. Ahlrichs, *Theor. Chem. Acc.* **1997**, *97*, 119-124.
[88] F. Weigend, R. Ahlrichs, *Phys. Chem. Chem. Phys*. **2005**, *7*, 3297-3305.
[89] F. Weigend, *J. Comput. Chem.* **2008**, *29*, 167-175.
[90] S. Grimme, S. Ehrlich, L. Goerigk, *J. Comput. Chem.* **2011**, *32*, 1456-1465.
[91] S. Grimme, J. Antony, S. Ehrlich, H. Krieg, *J. Chem. Phys.* **2010**, *132*, 154104.
[92] D. Andrae, U. Huermann, M. Dolg, H. Stoll, H. Preu, *Theoretica Chim. Acta* **1990**, *77*, 123-141.
[93] TURBOMOLE V7.3 2018, a Development of University of Karlsruhe and Forschungszentrum Karlsruhe GmbH, 1989-2007, TURBOMOLE GmbH, since 2007; Available from Http://Www.Turbomole.Com.
[94] L. F. Chibotaru, L. Ungur, *J. Chem. Phys.* **2012**, *137*, 064112.
[95] L. Ungur, L. F. Chibotaru, *Chem. Eur. J.* **2017**, *23*, 3708-3718.
[96] F. Aquilante, J. Autschbach, R. K. Carlson, L. F. Chibotaru, M. G. Delcey, L. De Vico, I. Fdez. Galván, N. Ferré, L. M. Frutos, L. Gagliardi, et al., *J. Comput. Chem*. **2016**, *37*, 506–541.
[97] B. O. Roos, R. Lindh, P. A. Malmqvist, V. Veryazov, P. O. Widmark, *J. Phys. Chem. A* **2004**, *108*, 2851-2858.
[98] B. O. Roos, R. Lindh, P. A. Malmqvist, V. Veryazov, P. O. Widmark, A. C. Borin, *J. Phys. Chem. A* **2008**, *112*, 11431-11435.
[99] W. Kutzelnigg, W. Liu, *J. Chem. Phys.* **2005**, *123*, 241102.
[100] D. L. Peng, M. Reiher, *Theor. Chem. Acc.* **2012**, *131*, 1081.
[101] M. Filatov, *J. Chem. Phys.* **2006**, *125*, 107101; discussion 107102.
[102] M. E. Lines, *J. Chem. Phys*. **1971**, *55*, 2977–2984.
[103] L. F. Chibotaru, L. Ungur, A. Soncini, *Angew. Chemie Int. Ed*. **2008**, *47*, 4126–4129.
[104] L. Ungur, W. Van den Heuvel, L. F. Chibotaru, *New J. Chem*. **2009**, *33*, 1224.
[105] L. F. Chibotaru, *in Mol. Nanomagnets Relat. Phenom*., **2014**, pp. 185–229.

10.1002/chem.201902837

WILEY-VCH

Entry for the Table of Contents

FULL PAPER

Intertwined effects: Triplet state position and metal coordination environment synergistically determine the properties of opto-magnetic lanthanide complexes. Both features are governed by the nature of the ligands. In a family of dinuclear terbium complexes, we show that the introduction of electron withdrawing groups in the ligand scaffold impacts the performance of the compounds in terms of photoluminescence quantum yield, luminescence thermometry and single-molecule magnet behaviour.

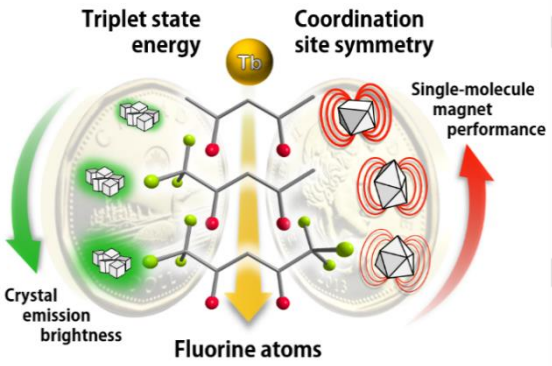

*Diogo A. Gálico‡, Riccardo Marin‡, Gabriel Brunet, Dylan Errulat, Eva Hemmer, Fernando A. Sigoli, Jani Moilanen, Muralee Murugesu**

Page No. – Page No.

Triplet state position and crystal field tuning in opto-magnetic lanthanide complexes: two sides of the same